Journal of the Korea Convergence Society
Vol. 8. No. 6, pp. 9-16, 2017
https://doi.org/10.15207/JKCS.2017.8.6.009

Autolanding Mission Planning of the IT Convergence Hoverable UAV

Sunghun Jung[1], Hyunsu Kim[2]
[1]Department of Drone System, Chodang University
[2]Department of Flight Operation, Chodang University

IT 융합 회전익 무인항공기의 자동 착륙 임무수행

정성훈[1*], 김현수[2]
[1]초당대학교 드론학과, [2]초당대학교 항공운항학과

Abstract Researchers are now faced with a limited flight time of the hoverable UAV due to the sluggish technological advances of the Li-Po energy density and try to find a bypassing solution for the fully autonomous hoverable UAV mission planning. Although there are several candidate solutions, automated wireless charging is the most likely and realistic candidate and we are focusing on the autolanding strategy of the hoverable UAV in this paper since it is the main technology of it. We developed a hoverable UAV flight simulator including Li-Po battery pack simulator using MATLAB/Simulink and UAV flight and battery states are analyzed. The maximum motor power measured as 1,647 *W* occurs during the takeoff and cell voltage decreases down to 3.39 *V* during the procedure. It proves that the two Li-Po battery packs having 22 *Ah* and connected in series forming 12S1P are appropriate for the autolanding mission planning.

• Key Words : Autolanding, Battery State Estimation, Hoverable UAV, Image Processing, SOC

요 약 Li-Po 에너지 밀도의 기술적 진보의 한계로 회전익 무인항공기의 비행시간은 제한적이기 때문에, 연구원들은 회전익 무인항공기의 완전한 자율 임무 수행을 위하여 우회 해결책을 찾고 있다. 몇 가지 후보 해결책들 중, 자동 무선 충전이 가장 가능성 있고 현실적인 후보이며, 본 논문에서는 자동 무선 충전의 주요 기술인 자동 착륙 전략에 초점을 맞추고 있다. MATLAB/Simulink를 기반으로 Li-Po 배터리팩 시뮬레이터를 포함한 회전익 무인항공기 비행 시뮬레이터를 개발하였으며, 이를 통해 비행 상태 및 배터리팩 상태를 분석하였다. 이륙할 때 1,647 *W*의 최대 모터 출력이 발생하였고, 이때 셀 전압은 최소 3.39 *V*까지 감소하였다. 이는 22 *Ah*를 지니고 12S1P로 연결된 2개의 배터리팩이 자동 착륙 임무수행에 적합하다는 것을 나타낸다.

• 주제어 : 자동착륙, 배터리 상태 추정, 회전익 무인항공기, 영상처리, 잔존용량

1. Introduction

Unmanned aerial vehicle (UAV) technologies are quite mature and mission planning like following multiple waypoints is widely being used without any difficulty. There are now many applications where a

UAV is put into for autonomous but limited mission performance, including filming, reconnaissance, rescue, fire extinguish, traffic monitoring, pesticide dusting, crop dusting, bridge inspection, wind turbine inspection, simultaneous localization and mapping (SLAM), fishing, and etc [1,2,3,4].

Although listed missions in the above are successfully demonstrated by using a UAV or sometimes using several UAVs, application of the UAV is constrained due to both HW and SW issues like low battery pack capacity, GPS spoofing, data hacking, and etc [5,6,7,8].

In particular, mission performance time is restricted to be around 10 to 30 *min* in case of a hoverable UAV due to the battery pack capacity. So, human operators need to be involved either to replace or to charge battery packs which is a very tiresome duty.

Several researchers try to automate battery pack replacement or charging procedures, but related technologies are at a rudimentary level at the moment and so there are not many real life applicable products [9,10,11].

To replace or charge battery packs of a UAV, the UAV firstly needs to approach to near the ground station (GS), detect the GS, descend flight altitude, land on the GS, and lastly be relocated to be precisely positioned to the replacement or charging system [12,13].

Among the listed automated procedures, we simulate procedures, including taking off from the GS, approaching to the GS, detecting the GS, descending the flight altitude, and landing on the GS, while we are monitoring the battery pack states [14,15,16].

From the simulation results, we could estimate how much of the battery pack capacity is consumed, how much of the battery pack temperature is increased, how much of the total motor power is required, whether the PID controller operates correctly, how accurately the UAV lands on the landing point, and etc.

These simulation results could be utilized by SW engineers to pre-analyze the autolanding flight behaviors of the newly designed algorithms. Also, system engineers could utilize the simulation results to select the optimum battery pack for the given autolanding mission.

The flow of this paper is as follows. Section 2 explains the governing models of the UAV and battery pack and Section 3 shows autolanding mission planning. Section 4 and Section 5 show simulation setup and corresponding results. Section 6 finally proposes the conclusion of this paper and future works.

2. Governing Model

A quadrotor dynamic model carrying two 6S1P battery pack models which are connected in series is used for the autolanding simulation.

2.1 UAV Model

Quadrotor dynamic model given in [17] and [Fig. 1] is adopted as

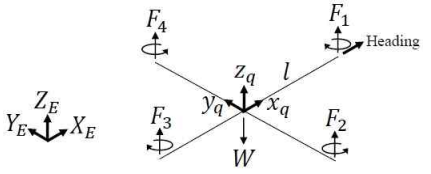

[Fig. 1] Quadrotor configuration

$$
\begin{aligned}
\ddot{x} &= (\cos\phi\sin\theta\cos\psi+\sin\phi\sin\psi)\frac{1}{m}b\left(w_1^2+w_2^2+w_3^2+w_4^2\right),\\
\ddot{y} &= (\cos\phi\sin\theta\sin\psi-\sin\phi\cos\psi)\frac{1}{m}b\left(w_1^2+w_2^2+w_3^2+w_4^2\right),\\
\ddot{z} &= (\cos\phi\cos\theta)\frac{1}{m}b\left(w_1^2+w_2^2+w_3^2+w_4^2\right)-g,\\
\ddot{\phi} &= \dot{\theta}\dot{\psi}\left(\frac{I_y-I_z}{I_x}\right)-\frac{J_r}{I_x}\dot{\theta}\left(w_1+w_3-w_2-w_4\right)+\frac{l}{I_x}b\left(w_4^2-w_2^2\right),\\
\ddot{\theta} &= \dot{\phi}\dot{\psi}\left(\frac{I_z-I_x}{I_y}\right)-\frac{J_r}{I_y}\dot{\phi}\left(w_1+w_3-w_2-w_4\right)+\frac{l}{I_y}b\left(w_1^2-w_3^2\right),\\
\ddot{\psi} &= \dot{\phi}\dot{\theta}\left(\frac{I_x-I_y}{I_z}\right)+\frac{l}{I_z}b\left(w_1^2+w_3^2-w_2^2-w_4^2\right),
\end{aligned}
\tag{1}
$$

where , , and are roll, pitch, and yaw angles (*rad*), is the UAV mass (*kg*), is the thrust factor (*no*

unit), w_i is the ith rotor speed (*rad/s*), g is the gravitational acceleration (m/s^2), I_x, I_y, and I_z are the body inertias ($kg \cdot m^2$), J_r is the propeller inertia ($kg \cdot m^2$), and l is the propeller length (*m*).

Then, we enhanced the Eq. 1 to use PID controllers as,

$$
\begin{aligned}
T &= k_p(z^* - z) + k_i \int_{t_1}^{t_2} (z^* - z)dt + k_d(\dot{z}^* - \dot{z}) + \sqrt{W/4b}, \\
\tau_x &= k_p(\phi^* - \phi) + k_i \int_{t_1}^{t_2} (\phi^* - \phi)dt + k_d(\dot{\phi}^* - \dot{\phi}), \\
\tau_y &= k_p(\theta^* - \theta) + k_i \int_{t_1}^{t_2} (\theta^* - \theta)dt + k_d(\dot{\theta}^* - \dot{\theta}), \\
\tau_z &= k_p(\psi^* - \psi) + k_i \int_{t_1}^{t_2} (\psi^* - \psi)dt + k_d(\dot{\psi}^* - \dot{\psi}),
\end{aligned}
\tag{2}
$$

where T is the sum of four rotor thrusts (*N*), k_p, k_i, and k_d are PID controller gains (*no unit*), W is the UAV weight (*N*), τ_x, τ_y, and τ_z are rolling, pitching, and yawing torques ($N \cdot m$), and uppercase letter $*$ represents reference data.

2.2 Battery Model

One ladder equivalent circuit model (ECM) shown in [Fig. 2] is adopted for the cell behavior simulation. Six of this cell ECM are connected in series to construct a pack and two separate pack models are connected in series.

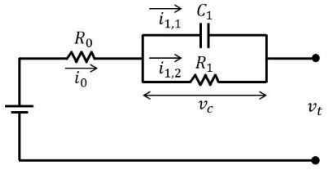

[Fig. 2] One ladder battery ECM

The state of charge (SOC) and open circuit voltage (OCV) can be estimated using the three parameters, , , and , in the cell ECM as

(3)

where v_c is the OCV (*V*), z is the SOC (%/100), $\triangle t$ is the step time (*s*) which is set as 0.1 *s*, τ_1 is the time constant (*s*) satisfying $\tau_1 = R_1 C_1$, η is the battery efficiency (assumed as 1), Q_{norm} is the current battery capacity (*Ah*), i_0 is the load current (*A*), n_v and n_z are the Gaussian noises (*V*), and the subscript k represents the present time index.

3. Autolanding Mission Planning

A quadrotor UAV (driven by a UAV model shown in Section 2.1 and powered by a battery model shown in Section 2.2) is maneuvered to take off at the location, [0, 0, 0], and land on the location, [5, 5, 1.1], where the GS is located.

The GS contains three GPS sensors at three tips of triangular shape bar and the UAV uses its data to approach the GS. Here, the length from the center to the each tip of the bar is 2 *m*.

Then, the UAV uses an image processing algorithm to detect marks attached to the top of the GS and recognizes it as the GS by using a camera attached at the bottom of the UAV. Mean location of the centers of the detected marks is used as the landing point. Here, the length of one side of a rectangle is 10 *cm*.

4. Simulation Setup

4.1 Quadrotor UAV

Specifications of the agricultural quadrotor UAV shown in <Table 1> and [Fig. 3] are used for the simulation [18,19,20].

<Table 1> Specifications of the quadrotor UAV

Wheelbase (*m*)	1.2

	Max. Cont.Current (*A*)	58
	Max. Cont. Power (*W*)	2,900
	Internal Resistance (Ω)	0.055
	Size (mm^3)	92 × 40
	Weight (g)	695
Total Flight Weight (*kg*)		24 (with 10 kg payload)
Flight Time (*min*)		10

[Fig. 3] Quadrotor UAV

4.2 Battery Pack

Quadrotor carries two Li-Po battery packs connected in series shown in [Fig. 4] and its specification is listed in <Table 2>.

[Fig. 4] Battery pack

<Table 2> Specifications of the battery pack

Manufacturer	Batterist
Serial Number	PQ-22000LP2
Configuration	6S1P
Voltage (*V*)	22.2
Capacity (*Ah*)	22
Cont. Max. C-rate (*C*)	18
Size (mm^3)	198 × 91 × 66

Environmental factors which affect battery pack behaviors are listed in <Table 3> to demonstrate the internal temperature change of the battery pack.

<Table 3> List of environmental factors

Convective Heat Transfer Coefficient (W/m^2K)	Between Cell and Cell	5
	Between Cell and Ambient Air	10
Volumetric Heat Capacity (J/m^3K)		2,040,000
Specific Heat (*J/kgK*)		404.3
Ambient Air Temperature (°C)		20

4.3 Simulink Model

Simulink, a graphical programming environment, is one of the widely used graphical block diagramming tools and is heavily used in the aerospace industry for the flight dynamics simulations.

Overall Simulink model is shown in [Fig. 5] and its operating configuration is shown in [Fig. 6].

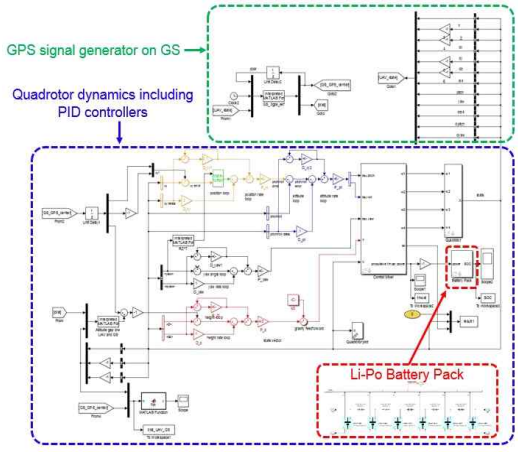

[Fig. 5] Overall Simulink model

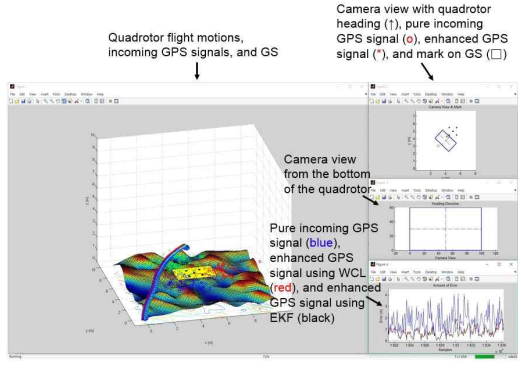

[Fig. 6] Operating configuration of the Simulink model

All simulations are performed with a quadrotor UAV carrying a battery pack having initial system properties as listed in <Table 4> and <Table 5>.

<Table 4> Initial system properties of UAV

P_{uav} (*m*)	[0, 0, 0]
v_{uav} (*m/s*)	[0, 0, 0]
a_{uav} (*m/s²*)	[0, 0, 0]
θ_{uav} (*rad*)	[0, 0, 0]
w_{uav} (*rad/s*)	[0, 0, 0]
$Altitude_{\min}$ (*m*)	25
$Altitude_{\max}$ (*m*)	30
$\| v_{uav,\min} \|_2$ (*m/s*)	0
$\| v_{uav,\max} \|_2$ (*m/s*)	20
$\| a_{uav,\min} \|_2$ (*m/s²*)	0
$\| a_{uav,\max} \|_2$ (*m/s²*)	10

<Table 5> Initial system properties of battery pack

SOC (%)	100
Capacity (*Ah*)	21.825 (at 20°C)
Temperature (°C)	20

Finally, a desktop used for simulations has the following system properties; Intel(R) Core(TM) i5-4590 CPU @ 3.30 GHz processor, 64-bit operating system, and 8.00 GB RAM.

5. Simulation Result

The total autolanding simulation takes about 12 s and simulation results of the UAV and battery pack are separately shown in the below.

5.1 Quadrotor UAV

Required motor power while the UAV takes off and lands on the GS is shown in [Fig. 7]. According to the result, the maximum motor power is 1,647 *W*.

During the flight, varying distance between the UAV and the GS is monitored and shown in [Fig. 8]. The maximum distance between the UAV and the GS turns out to be 3.54 *m*.

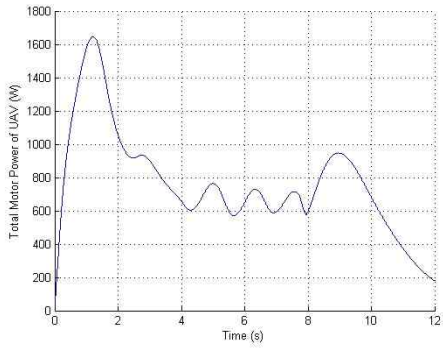

[Fig. 7] Total Motor Power vs. Time

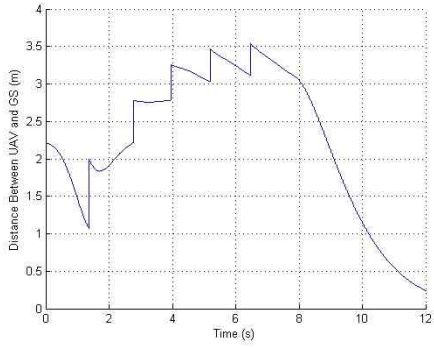

[Fig. 8] Distance between UAV and GS vs. Time

5.2 Battery Pack

Two battery packs which are connected in series are used as the UAV power source. Each battery pack consists of six cells connected in series and one pack is monitored during the autolanding simulation as shown in [Fig. 9], [Fig. 10], and [Fig. 11].

According to the result, the minimum cell voltage reaches 3.39 *V*, the maximum SOC consumption is 0.52 %, and the maximum cell temperature increases up to 20.9°C.

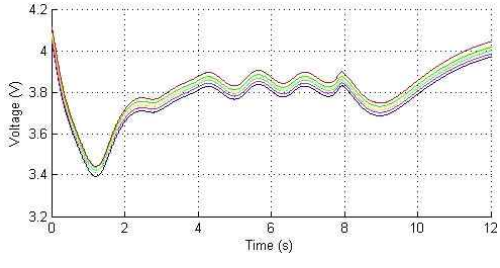

[Fig. 9] Cell voltage vs. Time

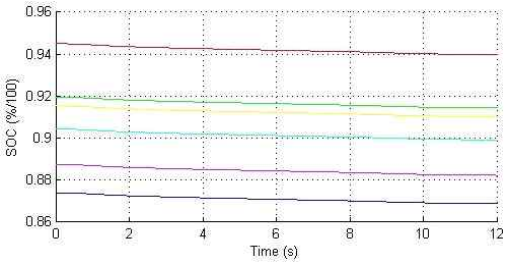

[Fig. 10] Cell SOC vs. Time

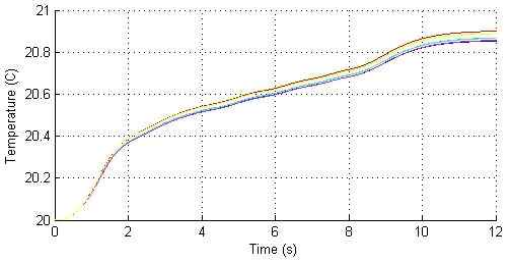

[Fig. 11] Cell temperature vs. Time

5.3 Flight Trajectory

The step-by-step autolanding flight trajectory is shown in [Fig. 12] and perspective and orthographic views of the trajectory are shown in [Fig. 12], [Fig. 13], and [Fig. 14]. Here, small circles with red, green, and blue colors represent pure incoming GPS data.

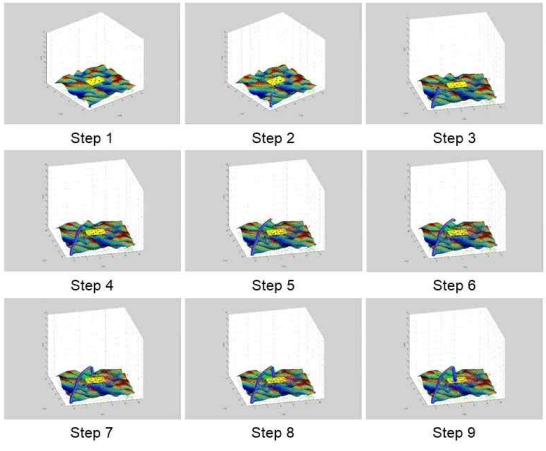

[Fig. 12] Step-by-step autolanding flight simulation

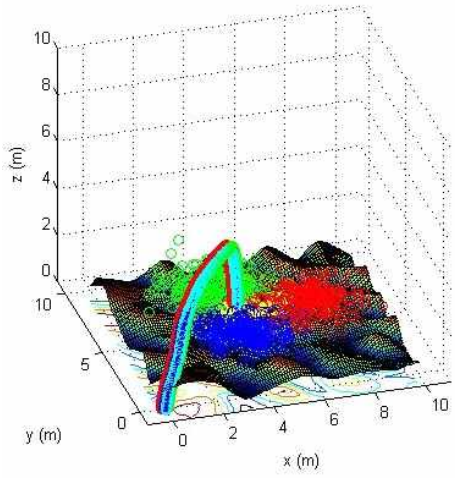

[Fig. 12] XYZ perspective view

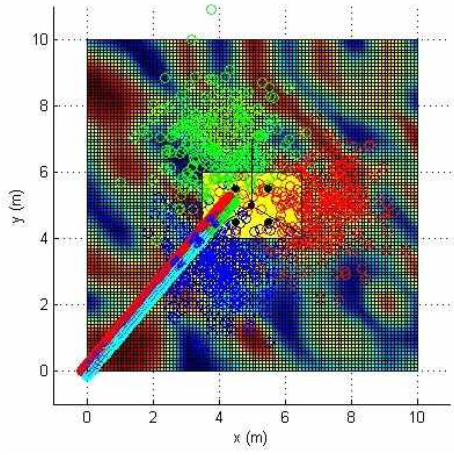

[Fig. 13] XY orthographic view

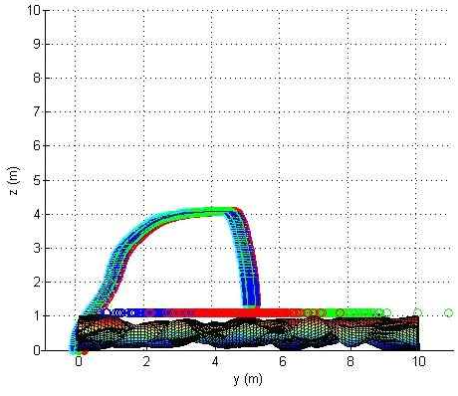

[Fig. 14] YZ orthographic view

6. Conclusion

Autolanding flight simulation of a quadrotor UAV is performed and state variation results of both the UAV and the battery pack are monitored for the analysis. According to simulation results, the minimum cell voltage, 3.39 *V*, is reached during the flight simulation and it shows two battery packs are suitable to manage well the total motor power of the UAV, 1,647 *W*, during the takeoff procedure.

We will utilize this autolanding simulation tool for the preliminary analysis during the design phase of the autonomous wireless charging GS in the future.

REFERENCES

[1] J. Lee, J. Lee, and K. Lee, "A Scheme of Security Drone Convergence Service using Cam-Shift Algorithm," Journal of the Korea Convergence Society, Vol. 7, No. 5, pp. 29-34, 2016.

[2] K. Kanistras, G. Martins, M. J. Rutherford, and K. P. Valavanis, "A Survey of Unmanned Aerial Vehicles (UAVs) for Traffic Monitoring," 2013 International Conference on Unmanned Aircraft Systems, pp. 221-234, 2013.

[3] B. McNeil and C. Snow, "The Truth about Drones in Mapping and Surveying," Skylogic Research, LLC, pp. 1-6, 2016.

[4] A. Restas, "Drone Applications for Supporting Disaster Management," World Journal of Engineering and Technology, Vol. 3, pp. 316-321, 2015.

[5] S. Kim and K. Lee, "User Authentication Risk and Countermeasure in Intelligent Vehicles," Journal of the Korea Convergence Society, Vol. 3, No. 1, pp. 7-11, 2012.

[6] J. Hong, "Threat Issues of Intelligent Transport System in the V2X Convergence Service Environment," Journal of the Korea Convergence Society, Vol. 6, No. 5, pp. 33-38, 2015.

[7] K. Lee and K. Lee, "Authentication Scheme using Biometrics in Intelligent Vehicle Network," Journal of the Korea Convergence Society, Vol. 4, No. 3, pp. 15-20, 2013.

[8] D. P. Shepard, T. E. Humphreys, and A. A. Fansler, "Evaluation of the Vulnerability of Phasor Measurement Units to GPS Spoofing Attacks," International Journal of Critical Infrastructure Protection, Vol. 5, Issues. 3-4, pp. 146-153, 2012.

[9] S. Jung, T. Lee, T. Mina, and K. B. Ariyur, "Inductive or Magnetic Recharging for Small UAVs," SAE Aerospace Electronics and Avionics Systems Conference, pp. 1-10, 2012.

[10] M. Valenti, D. Dale, J. P. How, and D. P. D. Farias, "Mission Health Management for 24/7 Persistent Surveillance Operations," Proceedings of the AIAA Guidance, Navigation, and Control Conference, pp. 1-18, 2007.

[11] K. A. O. Suzuki, P. K. Filho, and J. R. Morrison, "Automatic Battery Replacement System for UAVs: Analysis and Design," Journal of Intelligent and Robotic Systems, Vol. 65, Issue. 1, pp. 563-586, 2012.

[12] K. A. Swieringa, C. B. Hanson, J. R. Richardson, J. D. White, Z. Hasan, E. Qian, and A. Girard, "Autonomous Battery Swapping System for Small-Scale Helicopters," IEEE International Conference on Robotics and Automation, pp. 1-6, 2010.

[13] F. P. Kemper, K. A. O. Suzuki, and J. R. Morrison, "UAV Consumable Replenishment: Design Concepts for Automated Service Stations," Journal of Intelligent and Robotic Systems, Vol. 61, Issue. 1, pp. 369-397, 2011.

[14] G. Xu, Y. Zhang, S. Ji, Y. Cheng, and Y. Tian, "Research on Computer Vision-Based for UAV Autonomous Landing on a Ship," Pattern Recognition Letters, Vol. 30, pp. 600-605, 2009.

[15] K. E. Wenzel, A. Masselli, and A. Zell, "Automatic Take Off, Tracking and Landing of a Miniature UAV on a oving Carrier Vehicle," Journal of Intelligent and Robotic Systems, Vol. 61, pp.

221-238, 2011.
[16] B. Herisse, T. Hamel, R. Mahony, and F. X. Russotto, “Landing a VTOL Unmanned Aerial Vehicle on a Moving Platform Using Optical Flow,” IEEE Transactions on Robotics, Vol. 28, No. 1, pp. 77-89, 2012.
[17] P. Corke, Robotics, Vision and Control: Fundamental Algorithms in MATLAB, Springer-Verlag Berlin Heidelberg, 2011.
[18] https://goo.gl/ijxT7M
[19] https://goo.gl/baB8H6
[20] https://goo.gl/Jxj24f

저자소개

정 성 훈(Sunghun Jung) [정회원]

- 2009년 8월 : 미네소타대학교 기계공학과 (공학학사)
- 2010년 12월 : 퍼듀대학교 기계공학과 (공학석사)
- 2013년 12월 : 퍼듀대학교 기계공학과 (공학박사)
- 2014년 1월 ~ 2016년 8월 : 삼성SDI 책임연구원
- 2016년 9월 ~ 현재 : 초당대학교 드론학과 조교수

<관심분야> : 무인항공기 자율기동, 에너지 효율적 경로 최적화, 배터리팩 상태예측 알고리즘 개발

김 현 수(Hyunsu Kim) [정회원]

- 2014년 2월 : 항공대학교 항공운항관리학과 (이학석사)
- 2017년 2월 : 항공대학교 항공운항관리학과 (이학박사 수료)
- 2013년 1월 ~ 2013년 12월 : Griffith Research Center 연구원
- 2015년 3월 ~ 현재 : 초당대학교 항공운항학과 조교수

<관심분야> : 항공운항, 공항관리, 조종교육